Tunneling resistance of double-barrier tunneling structures with an alkanethiol-protected Au nanoparticle

H. Zhang* and Y. Yasutake
Department of Physical Electronics, Tokyo Institute of Technology, Tokyo 152-8552, Japan

Y. Shichibu and T. Teranishi†
School of Materials Science, Japan Advanced Institute of Science and Technology, 1-1 Asahidai, Tatsunokuchi, Nomi, Ishikawa 923-1292, Japan

Y. Majima‡
Department of Physical Electronics, Tokyo Institute of Technology and SORST, Japan Science and Technology Agency, Tokyo 152-8552, Japan

(Received 22 November 2004; revised manuscript received 6 September 2005; published 29 November 2005)

Coulomb staircases in double-barrier tunneling junctions consisting of a scanning-probe–vacuum-gap–alkanethiol-protected Au nanoparticle/Au (111) electrode have been measured as a function of the set point current of scanning tunneling spectroscopy. The tunneling resistances of the scanning probe-Au core of a nanoparticle (R_1) and the Au core-Au (111) electrode (R_2) are evaluated by fitting a theoretical Coulomb staircase into the experimental tunneling current-voltage characteristics measured by scanning tunneling spectroscopy. When a vacuum gap exists between the scanning probe and alkanethiol Au nanoparticles, R_1 is inversely proportional to the set point current. On the contrary, in the case of $R_1 < R_2$, the top of the tip of the scanning probe tends to penetrate the octanethiol-protecting molecule of an Au nanoparticle. R_2 is found to be independent of the set point current, and R_2 of octanethiol- and hexanethiol-protected Au nanoparticles are evaluated as 7.6 G$\Omega \pm 10\%$ and 460 M$\Omega \pm 10\%$, respectively.

DOI: 10.1103/PhysRevB.72.205441 PACS number(s): 73.23.Hk, 81.07.−b, 07.79.Cz

I. INTRODUCTION

Over the last few years, nanomechanical single electron systems have attracted significant fundamental and technological interests for applications in nanoelectronic devices.[1–8] In 1998, Gorelik *et al.* proposed the electron shuttle model based on nanomechanical double-barrier tunneling junctions (DBTJs), in which the polarity of a number of electrons on the Coulomb island can be controlled by the two tunneling resistances between the Coulomb island and two reservoirs.[4] In the DBTJ structure, single electron shuttle phenomena based on the self-excitation process will be observed if the Coulomb island can be vibrated by the charges on the island and the tunneling resistance ratio R_1/R_2 of the two junctions inverses due to the nanomechanical vibration. The design of the tunneling resistances in the nanomechanical single electron system is one of the most basic and important objectives to realize the single electron shuttle with self-excitation.

Only a few instances of electromechanical couplings have been experimentally reported in the studies of single electron systems.[5,9,10] Recently, we have demonstrated the electron shuttle motion by measuring the displacement and tunneling currents in nanomechanical DBTJs using a scanning vibrating probe.[11–16] However, it is still a challenge to fabricate a nanomechanical single electron system with self-excitation and to demonstrate the self-excited single electron shuttle motion experimentally.

Metallic nanoparticles protected by monolayer organic molecules have a wide range of applications as potential electronic components in nanoelectronic devices.[17,18] Alkanethiol-protected Au nanoparticles are one of the most fundamental capped nanoparticles,[19,20] in which the alkanethiol-protecting molecule can behave as a part of the tunneling barrier having mechanical flexibility.

The transconductance of the alkanethiol molecule have been studied by several methods, such as a Hg junction, a solid metal-insulator-metal junction, conductive contact atomic force microscopy, an electrochemical method, and scanning tunneling microscopy (STM).[21–27] The tunneling resistance of a two-layer tunnel junction, consisting of a vacuum and an alkanethiol self-assembled monolayer (SAM), has been reported.[23,28] The tuning of tunneling resistances and capacitances of DBTJs consisting of a STM-probe–vacuum–alkanethiol-protected Au nanoparticle-SAM-Au (111) substrate has also been performed by adjusting the STM set point current.[27] It should be noted that the tunneling resistances between the Au (111) substrate and the Au core of the alkanethiol-protected Au nanoparticles can be controlled by changing the length of alkanethiol. However, more detailed experiments are required to design the structure in a subnanometer scale in order to realize the electron shuttle with self-excitation.

In this paper, we demonstrate Coulomb staircases in the current-voltage characteristics of the DBTJ structures consisting of a scanning-probe–vacuum–alkanethiol-protected Au nanoparticle-Au (111) substrate by changing the set point current of scanning tunneling spectroscopy (STS). Theoretical Coulomb staircase curves have been fitted into the experimental results by introducing the full "orthodox" theory.[2,29,30] Two parameters were mainly evaluated, namely,

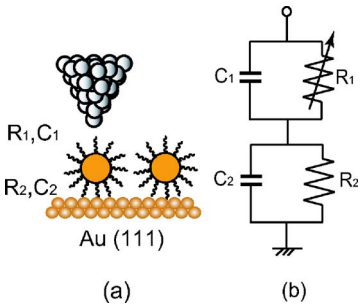

FIG. 1. (Color online) (a) Schematic drawing and (b) equivalent circuit of the nanomechanical double-barrier tunneling structure.

the tunneling resistance of the junctions R_1 between the probe and the Au core of the nanoparticle and the resistance R_2 between the Au core of the nanoparticle and the Au(111) substrate. The tunneling resistance ratios (R_1/R_2) of octanethiol (C8S)-protected and hexanethiol (C6S)-protected Au nanoparticles are discussed on the basis of the set point current.

II. EXPERIMENTAL

The synthesis of alkanethiol-protected Au nanoparticles is described elsewhere.[19,31] The diameters of C8S- and C6S-protected Au cores are controlled and estimated as approximately 2.4 ± 0.5 nm and 2.1 ± 0.5 nm, respectively, from a transmission electron microscopy (TEM) image. The lengths of protecting molecules are estimated as 1.44 and 1.18 nm for C8S and C6S, respectively.[32] As a result, the entire diameters of nanoparticles including the protecting alkanethiols and the Au core are estimated to be 5.3 ± 0.5 and 4.8 ± 0.5 nm for C8S- and C6S-protected Au nanoparticles, respectively. The dielectric constant of alkanethiol has been reported as 2.6.[33,34]

The Au substrate is prepared on cleaved mica by a vacuum evaporation method. After the evaporation, the Au substrate is heated at 450 °C for $6\sim7$ h to form an atomically flat Au (111) surface. Droplets of toluene solution containing C8S- and C6S-protected Au nanoparticles are spread on the Au (111)/mica substrate, and the solution is allowed to evaporate at room temperature.

The tunneling current-voltage characteristics are measured by the ultrahigh vacuum (UHV) low-temperature STM (Unisoku, USM-501) at 68 K. Figure 1 illustrates the idealized geometry and equivalent circuit of the nanomechanical DBTJ described in our work, which consists of an STM-probe–vacuum–alkanethiol-Au nanoparticle–Au (111) substrate. When a vacuum gap exists between the top of the STM probe and alkanethiol-protected Au nanoparticle, the tunneling resistance R_1 between the probe and the nanoparticle can be varied by adjusting the set point current, while the resistance R_2 between the nanoparticle and the Au(111) substrate depends on the alkanethiol-protecting molecule. In this paper, the set point current I_{set} is defined as the tunneling current at a bias voltage of −2 V and is varied from 1 to 800 pA.

III. RESULTS

Figures 2(a) and 2(b) show the STM images of C8S- and C6S-protected Au nanoparticles on the Au (111) surface at a

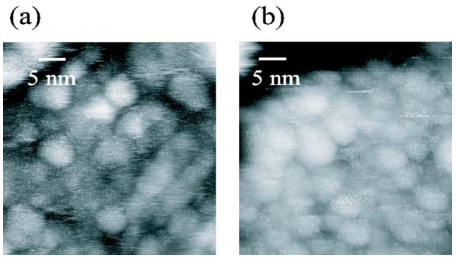

FIG. 2. (Color online) STM images of (a) C8S-protected and (b) C6S-protected Au nanoparticles on Au(111) substrates at a set point current of 3 pA and a probe bias voltage of −2 V. Scan size is 40 nm × 40 nm.

set point current of 3 pA and a probe voltage of −2 V. The packing structure of nanoparticles is observed in these images. In the case of both C8S-protected [Fig. 2(a)] and C6S-protected [Fig. 2(b)] Au nanoparticles, the typical diameter of a single nanoparticle in the STM images is approximately 4–5 nm, which corresponds to the entire size of a nanoparticle including the Au core and alkanethiol molecules. The diameters in the STM image are in good agreement with the estimated diameters of 5.3 ± 0.5 and 4.8 ± 0.5 nm for the C8S- and C6S-protected Au nanoparticles, respectively.

Figure 3 shows the normalized capacitance $C/4\pi\epsilon r$ as a function of the normalized distance (x/r) in a mirror image point-charge model of a charged sphere (radius r) at the distance x below a conducting plate.[12,35] It should be noted that the capacitance C is proportional to $4\pi\epsilon r$ that is equal to the capacitance of the sphere with the radius r in a free space. C decreases with increasing the distance x.

According to the full "orthodox" theory for the two junction system, the tunneling rate for the jth junction $\Gamma_j^{\pm}(n)$, where the $\pm$ refers to the forward or reverse tunneling process across the junctions ($n\rightarrow n\pm1$), can be obtained from a basic golden-rule calculation.[29,30]

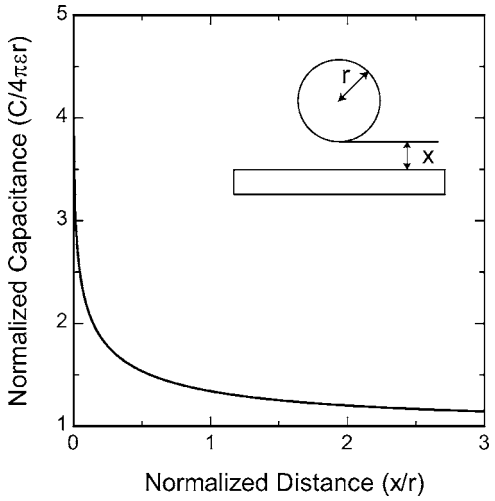

FIG. 3. Theoretical normalized capacitance $C/4\pi\epsilon r$ as a function of the normalized distance (x/r) in a mirror image point-charge model of a charged sphere (radius r) at the distance x below a conducting plate.

$$\Gamma_j^{\pm}(n) = \frac{1}{R_j e^2}\left(\frac{-\Delta E_j^{\pm}}{1-\exp(\Delta E_j^{\pm}/k_B T)}\right), \tag{1}$$

where $\Delta E_j^{\pm}$ is the energy change of the system when the electron tunnels across the barrier. $\Gamma_j^{\pm}(n)$ is inversely proportional to the tunneling resistance. The equations for $\Delta E_j^{\pm}$ are obtained from electrostatic energy considerations ($e>0$).

$$\Delta E_1^{\pm} = \frac{e}{C_1+C_2}\left(\frac{e}{2} \pm (ne-Q_0) \mp C_2 V\right),$$
$$\Delta E_2^{\pm} = \frac{e}{C_1+C_2}\left(\frac{e}{2} \pm (ne-Q_0) \pm C_1 V\right), \tag{2}$$

where C_1 is the capacitance between the probe and the Au core of the nanoparticle, C_2 is the capacitance between the Au core of the nanoparticle and the Au(111) substrate, and Q_0 is the fractional residual charge ($|Q_0| \leqslant e/2$). Then the ensemble distribution of the number of electrons on the nanoparticle $\sigma(n)$ is obtained by noting that the net probability for making a transition between any two adjacent states in steady state is zero as

$$\sigma(n)[\Gamma_1^+(n)+\Gamma_2^+(n)] = \sigma(n+1)[\Gamma_1^-(n+1)+\Gamma_2^-(n+1)]. \tag{3}$$

Since $\Gamma_j^{\pm}$ are known from Eqs. (1) and (2), $\sigma(n)$ can be solved by subjecting to the normalization condition $\Sigma_{n=-\infty}^{\infty}\sigma(n)=1$. Tunneling current is then given by

$$I(V) = e\sum_{n=-\infty}^{\infty} n\sigma(n)[\Gamma_2^-(n)-\Gamma_2^+(n)]$$
$$= e\sum_{n=-\infty}^{\infty} n\sigma(n)[\Gamma_1^+(n)-\Gamma_1^-(n)]. \tag{4}$$

As a consequence, the theoretical $I(V)$-V curves can be numerically obtained.

Figure 4 shows typical theoretical normalized tunneling current $[I(V)R_1]$-probe bias voltage V dependence for various tunneling ratios R_1/R_2 in the range from 1 to 1000 with $R_2=10$ GΩ, $C_1=0.18$ aF, $C_2=0.20$ aF, and $Q_0=0.1e$ at 68 K. The theoretical $I(V)R_1$ curves show the Coulomb staircase and the conductance quantization gradually disappears on decreasing the ratio R_1/R_2. The value of the tunneling resistances of R_1 and R_2 are explained as follows. In the case of $1<R_1/R_2<50$, the shape of the theoretical normalized tunneling current $I(V)R_1$ curves strongly depend on the ratio R_1/R_2 especially in the probe voltage range between the onset of the first Coulomb step at the positive and the negative probe voltages. On the contrary, as the ratio R_1/R_2 is larger than 50 ($R_1 \gg R_2$), $I(V)R_1$ curves show clear the Coulomb staircase and become independent of R_1/R_2. It should be noted that the slope of a tangential line of theoretical $I(V)R_1-V$ curve tends to proportional to $R_1/(R_1+R_2)$ due to the Ohm's law. As a result, the total tunneling resistance of R_1+R_2 can be estimated by the reciprocal value of the tangential line. The ratio of R_1/R_2 is discussed in detail in the next section.

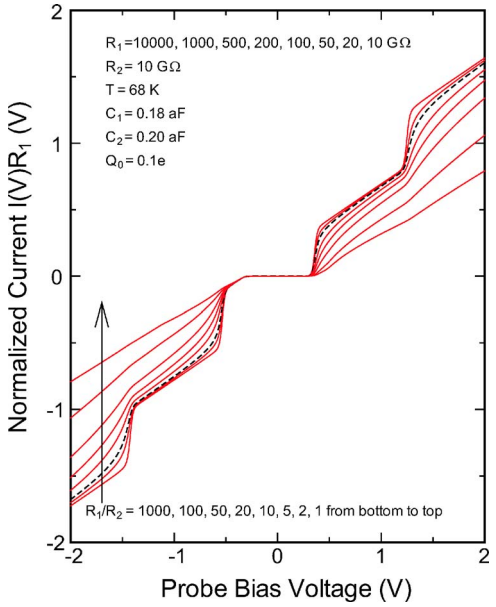

FIG. 4. (Color online) Theoretical normalized $I(V)R_1$ curves as a function of the tunneling resistance ratio R_1/R_2 where R_1/R_2 are 1000, 100, 50, 20, 10, 5, 2, 1, assuming $R_2=10$ GΩ, $C_1=0.18$ aF, $C_2=0.20$ aF, and $Q_0=0.1e$ at 68 K.

Figures 5 show typical experimental Coulomb staircases (solid lines) for C8S-protected Au nanoparticles [Figs. 5(a)–5(c)] at the set point currents of 6, 15, and 300 pA, and for C6S-protected Au nanoparticles [Figs. 5(d) and 5(e)] at the set point currents of 15 and 400 pA, respectively. Considering the small set point current such as 6 and 15 pA, clear Coulomb staircases have been observed for all the measurements. It should be noted that when the probe voltage becomes higher than ±1.5 V, the tunneling currents tend to increase steeply and deviate from the theoretical curves, suggesting a change in the tunneling process from direct tunneling to Fowler-Nordheim (FN) tunneling.[25]

IV. DISCUSSIONS

In this section, we discuss the possibility of independently controlling the tunneling resistances R_1 and R_2 toward the design of the nanomechanical DBTJ on the basis of a decay constant and an effective contact area. As shown in Fig. 4, the total tunneling resistance of R_1+R_2 can be estimated from the tangential line of the experimental Coulomb staircase, however, the estimation of individual value of R_1 and R_2 should require the consideration of the values of C_1, C_2, and Q_0. As the Au nanoparticles are protected by octanethiol C8S or hexanethiol C6S, C_1 should become smaller than C_2 when there exists a vacuum gap between the tip and the nanoparticle.

As a result, the distance of a vacuum gap between the tip and the nanoparticle (d_{gap}) is important to decide C_1 and C_2. Bumm *et al.* have estimated the transconductance of the alkanethiol molecule by the STM image of the mixed composition of SAM[28] and dodecanethiol on Au(111).[23] They introduced the two-layer tunnel junction model that composed of

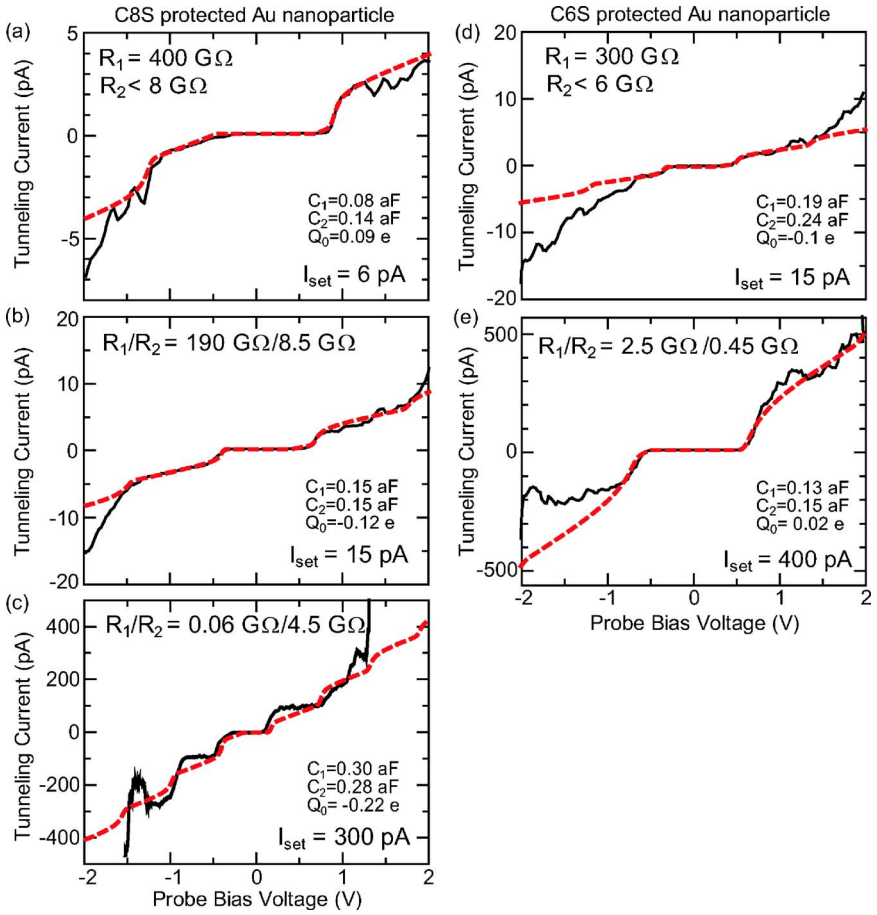

FIG. 5. (Color online) Typical Coulomb staircases of tunneling current versus voltage (solid line) at set point currents of (a) 6 pA, (b) 15 pA, and (c) 300 pA for C8S-protected Au nanoparticles; and (d) 15 pA and (e) 400 pA for C6S-protected Au nanoparticle, respectively. Dashed lines represent the theoretical curves. The I-V curves of (a), (b), and (c) are obtained from different C8S-protected Au nanoparticles of the same sample, and those of (d) and (e) are obtained from different C6S-protected Au nanoparticles of the other sample.

two distinct layers of the alkanethiol SAM and a vacuum gap, and suggested the decay constant of the alkanethiol SAM as 1.2 $Å^{-1}$ which corresponds that the transconductance of the decanethiol SAM is one order higher than that of the dodecanethiol SAM. We have also reported the direct measurements of the tunneling resistances of octanethiol (C8S) and hexanethiol (C6S) SAMs on Au (111) substrate by the tunneling current (I) distance (d) dependence between the STM probe and alkanethiol SAMs on the Au (111) substrate. The decay constant of the alkanethiol SAMs (α) and a vacuum (β) are estimated as 1.2 $Å^{-1}$ and 2.0 $Å^{-1}$, respectively, at a probe voltage of −2 V,[28] suggesting good agreement with the hypothetical results of Bumm *et al.*

Assuming that the transresistance between the tip and the Au core of the nanoparticle is obtained based on the two-layer junction model of the tip/vacuum/alkanethiol SAM/Au(111) substrate, the transresistance between the tip and the Au (111) substrate is given by $R=R_0 \exp(\beta d_{\mathrm{gap}})$, where the prefactor R_0 is respective contact resistance. For example, R becomes $1000R_0$, when there exists a vacuum gap of $d_{\mathrm{gap}}=0.35$ nm under the decay constant of $\beta=2.0$ $Å^{-1}$.

Considering the radius r of Au cores (1.2±0.3 nm and 1.1±0.3 nm for C8S and C6S), the lengths of protecting molecules (1.44 and 1.18 nm for C8S and C6S), and the dielectric constant of the alkanethiol (2.6), the change in C due to the vacuum gap should be small. For example, as shown in Fig. 3, the value of C decreases only 15% from $x=1$ to 3 nm under the diameter of 2 nm ($r=1$ nm).

In the case of $R_1/R_2>1$, the capacitance C_1 can be obtained by the Coulomb step in the current at equal voltage spacing of e/C_1. As discussed above, the value of C_2 should become in the range between C_1 and $1.2C_1$. The fractional residual charge Q_0 may either vanish or offset the Coulomb blockade. It should be noted that Q_0 is extremely sensitive to changes in the electrostatic environment such as electron tunneling to the neighboring Au nanoparticles.[36] As shown in Fig. 4, the zero-current region depends on C_1, C_2, and Q_0, however, not on R_1/R_2. On the other hand, as the shape of the first Coulomb step directly depends on the ratio R_1/R_2, both R_1 and R_2 can be estimated individually. Consequently, the fitting procedure is applied to the probe voltage range between the onset of the first Coulomb step at the positive and the negative probe voltages to avoid the charging effect to the neighboring Au nanoparticles, and the fitting parameters of R_1, R_2, C_1, C_2, and Q_0 are obtained. In Figs. 5, the dashed lines represent the theoretical curves obtained by the fitting procedure. The theoretical curves are in good agreement with the experimental results of the probe voltage range of the onset of the first Coulomb steps. It should be noted that R_2 cannot be estimated as an unique value in the case of $R_1/R_2 \geqslant 50$, since the shape of $I(V)R_1$ curves are independent of the ratio R_1/R_2 around the onset of the first Coulomb steps. In the case of $R_1/R_2<1$, the same fitting procedure can be applied by exchanging the subscripts 1 and 2 of the resistances and capacitances.

Figures 6(a) and 6(b) show the set point current (I_{set}) dependence of R_1 and R_2, respectively, which are evaluated by

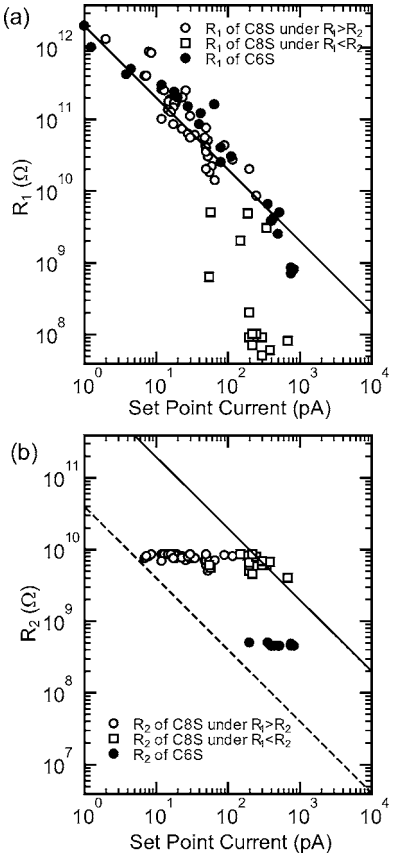

FIG. 6. Set point current dependence of tunneling resistances (a) R_1 and (b) R_2 for C8S- and C6S-protected Au nanoparticles. Open circles represent C8S-protected Au nanoparticle in the region of $R_1 > R_2$, open squares represent C8S-protected Au nanoparticles in the region of $R_1 < R_2$, and closed circles represent C6S-protected Au nanoparticles. (a) Solid lines indicate the power law of $R_1 \propto I_{set}^{-1}$ under $I_{set}R_1 = -2$ V as $V_{set} = -2$ V. In (b), the solid and the dashed lines show the power law relationship of $I_{set}R_1 = -2$ V and $I_{set}R_2 = -0.04$ V ($R_1/R_2 = 50$), respectively. The values of R_2 estimated in the area above the dashed line are shown in (b). The average values of R_2 for C8S- and C6-protected Au nanoparticles are 7.6 GΩ ± 10% and 460 MΩ ± 10% with the core sizes of ~2.4 nm and ~2.1 nm, respectively.

fitting the theoretical curves into the experimental Coulomb staircases. It should be noted that the fitting parameters of C8S and C6S data are estimated from the collections of $I(V)$-V curves obtained from different nanoparticles on the same C8S and C6S samples, respectively. In Figs. 6(a) and 6(b), R_1 of C8S-protected Au nanoparticles can be classified into two ranges $R_1 > R_2$ and $R_1 < R_2$. On the other hand, the tunneling resistances of C6S-protected Au nanoparticles are always $R_1 > R_2$ in the set point current range between 1 and 800 pA. When R_1 dominates the total resistance, R_1 should be inversely proportional to the set point current in the range of $R_1 > R_2$. The solid line in Fig. 6(a) shows the power law of $R_1 \propto I_{set}^{-1}$ under the set point current measurement condition of $I_{set}R_1 = -2$ V as the set point probe voltage V_{set} of −2 V. It should be noted that the evaluated results of I_{set} dependence of R_1 are in good agreement with the power law for both C8S- and C6S-protected Au nanoparticles. In Fig. 6(b), the

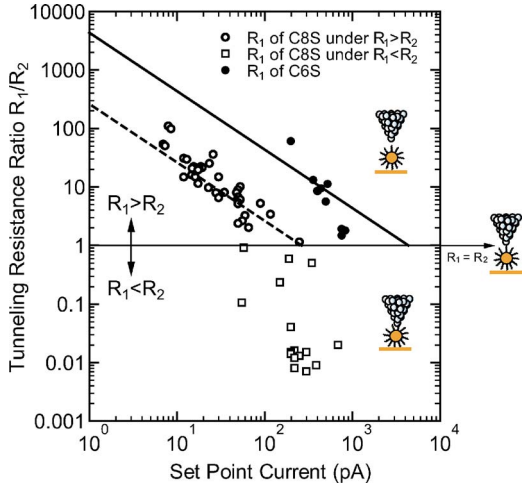

FIG. 7. (Color online) Set point current dependence of tunneling resistance ratio R_1/R_2. Open circles represent C8S-protected Au nanoparticles in the region of $R_1 > R_2$, open squares represent C8S-protected Au nanoparticle in the region of $R_1 < R_2$, and closed circle represent C6S-protected Au nanoparticle. The dashed and solid lines show the power law relationship of $I_{set}R_1/R_2 = -260$ pA($= V_{set}/R_2 = -2$ V/7.6 GΩ) and $I_{set}R_1/R_2 = -4.3$ nA($= V_{set}/R_2 = -2$ V/460 MΩ) for C8S- and C6S-protected Au nanoparticles, respectively. The insets provide the schematic DBTJ structures corresponding to the values of R_1/R_2.

solid and the dashed lines show the power law relationship of $I_{set}R_1 = -2$ V [as the same in Fig. 6(a)] and $I_{set}R_2 = -0.04$ V ($R_1/R_2 = 50$), respectively. If the value of R_2 is placed on the dashed line, R_1/R_2 becomes 50. As shown in Fig. 4, $I(V)$ curves are independent of R_1/R_2 in the case of $R_1/R_2 > 50$. As a result, R_2 can be obtained in the area above the dashed line in Fig. 6(b). R_2 of C8S-protected and C6S-protected Au nanoparticles under the ratio range of $1 < R_1/R_2 < 50$ are found to have constant values of 7.6 GΩ ± 10% and 460 MΩ ± 10%, respectively.

Figure 7 shows the set point current dependence of the tunneling resistance ratio (R_1/R_2) for C8S- and C6S-protected Au nanoparticles. The dashed and solid lines show the power law relationship of $I_{set}R_1/R_2 = -260$ pA ($= V_{set}/R_2 = -2$ V/7.6 GΩ) and $I_{set}R_1/R_2 = -4.3$ nA($= V_{set}/R_2 = -2$ V/460 MΩ) for C8S- and C6S-protected Au nanoparticles, respectively. As shown in Figs. 6(a) and 6(b), the tunneling resistance ratio (R_1/R_2) is also separated into two regions by the boundary value of $R_1/R_2 = 1$. According to the DBTJ structure in Fig. 1, this boundary value suggests a symmetric structure, i.e., the probe is just in contact with the end group of the alkanethiol-protecting molecule.

As the resistance tends to depend on the area of the tunneling junction, it is important to take into account the effective contact area. Wang *et al.* have estimated a resistance between a heptanethiol-protected Au nanoparticle and Au(111) consisting of an Au-core–heptanethiol-protecting-molecule–decanethiol SAM/Au(111).[27] They suggested the resistance as 69 MΩ with the core size of ~15 nm. We find that R_2 is independent of the set point current and nanoparticles in the region of $R_1/R_2 > 1$, and the average R_2 values of C8S- and C6S-protected Au nanoparticles are estimated as

7.6 GΩ and 460 MΩ with the core sizes of ~2.4 and ~2.1 nm as shown in Fig. 6(b), respectively. The average R_2 value of C8S is almost one order of magnitude higher than that of C6S, and the R_2 errors of C8S and C6S are within ±10%. It should be noted that the R_2 values of the protecting molecules of C8S and C6S are the same orders with the tunneling resistances of C8S and C6S SAMs which values were measured by the tunneling current (I)-distance (d) dependence.[28] Comparing the values of R_2 in this paper with the resistance in Wang's paper,[27] the effective contact area should be found to strongly depend on the core size. As a consequence, in the case of the Au core diameter of approximately 2 nm, the tunneling resistance between the Au core and the Au(111) substrate tends to become almost same value of the individual alkanethiol molecules in SAM on Au(111) and can be controlled by the length of the alkanethiol-protecting group in the Au nanoparticle.

Since the tunneling resistance R_2 between the Au core and Au (111) substrate is independent of the set point current, the tunneling resistance ratio R_1/R_2 is also inversely proportional to the set point current I_{set} for both C6S-Au and C8S-Au nanoparticles in the region of $R_1/R_2>1$, as shown in Fig. 7. At the same value of I_{set}, it is found that the approximately one order of difference in R_1/R_2 between the C8S- and C6S-protected Au nanoparticles is completely due to the difference in R_2 between the octanethiol- and hexanethiol-protecting molecules.

As shown in Fig. 6(a), the value of R_1 for C8S-protected Au nanoparticles tends to steeply decrease by several orders of magnitude within the set point current I_{set} range of 50 ~700 pA. On the contrary, the value of R_2 tends to remain constant in the range of $R_1<R_2$ [Fig. 6(b)]. As a result, the top of the tip of the scanning probe should penetrate the C8S-protecting molecule of Au nanoparticles; however, the distance between the Au core and the Au(111) substrate is still maintained to a large extent by C8S-protecting molecules, as illustrated in Fig. 7. On the other hand, in the case of the C6S-protected Au nanoparticle, the tunneling resistance ratio R_1/R_2 is always larger than 1; I_{set} is as high as 800 pA due to the small R_2.

In summary, the salient points for realizing the design of the nanomechanical DBTJ structures are as follows: the values of the tunneling resistances of the octanethiol- and hexanethiol-protecting molecules are 7.6 GΩ±10% and 460 MΩ±10% with the core sizes of ~2.4 and ~2.1 nm, respectively, which are of the same order as the individual octanethiol and hexanethiol molecules in SAMs on Au (111) substrates, respectively. The tunneling resistances of the alkanethiol-protecting molecule can increase by one order by using an alkanethiol having two extra methylene units in the case of the core diameter of approximately 2 nm. The top of the scanning probe tends to be in slight contact with the end group of the C8S- and C6S-protecting molecules at approximately 300 pA and 3 nA, respectively (Fig. 7). Considering the decay constants of a vacuum (2.0 $Å^{-1}$) and alkanethiol (1.2 $Å^{-1}$),[28] a vacuum gap between the probe and the alkanethiol-protecting molecule for the C6S-protected Au particle is only 0.1 nm longer than that for the C8S-protected Au nanoparticle at the same set point current. In the region of $R_1/R_2>1$, R_1 is inversely proportional to the set point current I_{set}. These results provide us with information that can be used to realize an electron shuttle with self-excitation.

V. CONCLUSION

The tunneling resistances of the scanning probe-Au core of the nanoparticle (R_1) and the Au core-Au (111) substrate (R_2) have been investigated by fitting the theoretical Coulomb staircases into the experimental I-V curves. The tunneling resistances of the octanethiol- and hexanethiol-protecting molecules have been evaluated as 7.6 GΩ±10% and 460 MΩ±10% with the core sizes of ~2.4 and ~2.1 nm, respectively, which indicates that R_2 become the same order as the individual octanethiol and hexanethiol molecules in SAMs on Au(111) substrates and can be controlled by changing the length of the alkanethiol-protecting molecules. These results are significant for designing the nanomechanical DBTJ structure by using alkanethiol molecules.

ACKNOWLEDGMENTS

This work is partially supported by the 21st Century COE Program, Photonics Nanodevice Integration Engineering by the Ministry of Education, Culture, Sports, Science and Technology (MEXT).

*Present address: School of Electronic and Information Engineering, Xi'an Jiaotong University, Xi'an Shaanxi, People's Republic of China.

†Present address: Graduate School of Pure and Applied Sciences, University of Tsukuba, 1-1-1 Tennodai, Tsukuba, Ibaraki 305-8571, Japan

‡Corresponding author: majima@pe.titech.ac.jp

[1] H. Grabert and M. H. Devoret, *Single Charge Tunneling: Coulomb blockade phenomena in nanostructures*, Vol. 294, NATO *Advanced Studies Institute* Series B, Physics, edited by H. Grabert and M. H. Devoret (Plenum Press, New York, 1992).

[2] L. L. Sohn, L. P. Kouwenhoven, and G. Schön, *Mesoscopic Electron Transport* (Kluwer, Boston, 1997).

[3] J. G. A. Dubois, J. W. Gerritsen, S. E. Shafranjuk, E. J. G. Boon, G. Schmid, and H. van Kempen, Europhys. Lett. **33**, 279 (1996).

[4] L. Y. Gorelik, A. Isacsson, M. V. Voinova, B. Kasemo, R. I. Shekhter, and M. Jonson, Phys. Rev. Lett. **80**, 4526 (1998).

[5] H. Park, J. Park, A. Lim, E. Anderson, A. Alivisatos, and P. McEuen, Nature (London) **407**, 57 (2000).

[6] A. Erbe, C. Weiss, W. Zwerger, and R. H. Blick, Phys. Rev. Lett. **87**, 096106 (2001).

[7] N. Nishiguchi, Phys. Rev. B **65**, 035403 (2001).

[8] R. I. Shekhter, Yu. Galperin, L. Y. Gorelik, A. Isacsson, and M. Jonson, J. Phys.: Condens. Matter **15**, R441 (2003).

[9] M. T. Tuominen, R. V. Krotkov, and M. L. Breuer, Phys. Rev.

Lett. **83**, 3025 (1999).
[10] Y. Majima, Y. Azuma, and K. Nagano, Appl. Phys. Lett. **87**, 163110 (2005).
[11] Y. Majima, S. Miyamoto, Y. Oyama, and M. Iwamoto, Jpn. J. Appl. Phys. **37**, 4557 (1998).
[12] Y. Majima, Y. Oyama, and M. Iwamoto, Phys. Rev. B **62**, 1971 (2000).
[13] Y. Majima, S. Uehara, T. Masuda, A. Okuda, and M. Iwamoto, Thin Solid Films **393**, 204 (2001).
[14] Y. Majima, K. Nagano, and A. Okuda, Jpn. J. Appl. Phys. **41**, 5381 (2002).
[15] K. Nagano, A. Okuda, and Y. Majima, Appl. Phys. Lett. **81**, 544 (2002).
[16] Y. Azuma, K. Nagano, and Y. Majima, Jpn. J. Appl. Phys. **42**, 2458 (2003).
[17] D. J. Schiffrin, Mater. Res. Bull. **26**, 1015 (2001).
[18] W. P. Wuelfing, A. C. Templeton, and R. W. Murray, Acc. Chem. Res. **33**, 27 (2000).
[19] T. Teranishi, S. Hasegawa, T. Shimizu, and M. Miyake, Adv. Mater. (Weinheim, Ger.) **13**, 1699 (2001).
[20] M. J. Hostetler, A. C. Templeton, and R. W. Murray, Langmuir **15**, 3782 (1999).
[21] R. E. Holmlin, R. Haag, M. L. Chabinyc, R. F. Ismagilov, A. E. Cohen, A. Terfort, M. A. Rampi, and G. M. Whitesides, J. Am. Chem. Soc. **123**, 5075 (2001).
[22] T. Lee, W. Wang, J. F. Klemic, J. J. Zhang, J. Su, and M. A. Reed, J. Phys. Chem. B **108**, 8742 (2004).
[23] L. A. Bumm, J. J. Arnold, T. D. Dunbar, D. L. Allara, and P. S. Weiss, J. Phys. Chem. B **103**, 8122 (1999).
[24] X. D. Cui, X. Zareate, J. Tomfohr, O. E. Sankey, A. Primak, A. L. Moore, T. A. Moore, D. Gust, G. Harris, and S. M. Lindsay, Nanotechnology **13**, 5 (2002).
[25] W. Wang, T. Lee, and M. A. Reed, Phys. Rev. B **68**, 035416 (2003).
[26] D. J. Wold and C. D. Frisbie, J. Am. Chem. Soc. **123**, 5549 (2001).
[27] B. Wang, H. Wang, H. Li, C. Zeng, J. G. Hou, and X. Xiao, Phys. Rev. B **63**, 035403 (2001).
[28] Y. Yasutake, Z. Shi, T. Okazaki, H. Shinohara, and Y. Majima, Nano Lett. **5**, 1057 (2005).
[29] A. E. Hanna and M. Tinkham, Phys. Rev. B **44**, 5919 (1991).
[30] D. V. Averin and K. K. Likharev, *Mesoscopic Phenomena in Solids*, edited by B. L. Altshuler, P. A. Lee, and R. A. Webb (Elsevier, Amsterdam, 1991), p. 169.
[31] T. Shimizu, T. Teranishi, S. Hasegawa, and M. Miyake, J. Phys. Chem. B **107**, 2719 (2003).
[32] N. Camillone, III, T. Y. B. Leung, P. Schwartz, P. Eisenberger, and G. Scoles, Langmuir **12**, 2737 (1996).
[33] M. D. Porter, T. B. Bright, D. L. Allara, and C. E. D. Chidsey, J. Am. Chem. Soc. **109**, 3559 (1987).
[34] M. A. Rampi, O. J. A. Schueller, and G. M. Whitesides, Appl. Phys. Lett. **72**, 1781 (1998).
[35] Y. Oyama, Y. Majima, and M. Iwamoto, J. Appl. Phys. **86**, 7087 (1999).
[36] C. T. Black, M. T. Tuominen, and M. Tinkham, Phys. Rev. B **50**, 7888 (1994).